Research Article

Received: 2 March 2013 Revised: 21 April 2013 Accepted article published: 2 May 2013 Published online in Wiley Online Library:

(wileyonlinelibrary.com) DOI 10.1002/jctb.4113

Kinetics of the liquid phase selective hydrogenation of 2,3-butanedione over new composite supported Pd catalysts

Nicolás Carrara,[a] Juan Badano,[a] Nicolás Bertero,[a,b] Gerardo Torres,[b] Carolina Betti,[a] Luciana Martínez-Bovier,[b] Mónica Quiroga[a,b] and Carlos Vera[a,b]*

Abstract

BACKGROUND: Heterogeneous hydrogenation catalysts for fine chemical synthesis are a convenient alternative to homogeneous catalysts because of the ease of separation and reuse. In order to be good catalysts they must have high activity and selectivity and good mechanical properties. Appropriate kinetic models should also be available for reactor design.

Novel composite supported Pd catalysts were synthesized and tested in the liquid-phase selective hydrogenation of 2,3-butanedione to 3-hydroxy-2-butanone (acetoin). The composite support comprised a mixture of an organic polymer and γ-Al_2O_3. The support and the Pd catalyst were further characterized by XRD, SEM, EMPA and XPS spectroscopy. Catalytic tests at various conditions were performed in order to elucidate the kinetics of the system.

RESULTS: The composite had better mechanical properties (resistance to radial and axial compression) in comparison with other commercial supports. Good activity and high selectivity to acetoin, a product of partial hydrogenation, were obtained at different reaction conditions. A Langmuir–Hinshelwood chemical rate expression useful for reactor design was regressed from the kinetic data.

CONCLUSIONS: The experimental results could be explained by a Horiuti–Polanyi mechanism in which the addition of an H atom to the carbonyl group in the adsorbed state is the rate limiting step.

Keywords: selective hydrogenation; 2,3-butanedione; acetoin; palladium; composite; kinetics

INTRODUCTION

In recent years the hydrogenation of dicarbonylic compounds to produce high value added products such as α-hydroxy-carbonyl compounds and α,β-diols has been especially studied.[1–3] The selective partial hydrogenation of 2,3-butanedione to 3-hydroxy-2-butanone (acetoin) or 2,3-dihydroxybutane is of special interest in the industry of flavors and fragrances.[4–7]

2,3-butanedione, most commonly known as diacetyl, is suspected to cause some health problems, especially in the respiratory system. *Bronchiolitis obliterans*, a severe lung disease has been detected in workers in the flavor industry.[6] For this reason in the USA and Europe, the use of diacetyl in this industry has been replaced by that of acetoin or acetyl propionyl.[7] Acetoin has low volatility and toxicity, its manipulation being therefore easier and healthier for laboratory and industry workers.

The exothermy of hydrogenation and the mass transfer problems raised by high reaction rates have led to the development of special supported metal catalysts with egg-shell distribution. This is of special importance for noble metal catalysts for which the onset of hot spots can lead to costly catalyst damage. In this sense we have previously reported the use of novel composite supports for the synthesis of improved egg-shell Pd hydrogenation catalysts.[8] These composite supports are formed by a mixture of an inorganic phase and an organic phase. The inorganic phase can be alumina, silica or other inorganic support and the organic phase is synthesized by mixing one or more organic monomers. These composite supports have been found to have better mechanical properties than commercial supports, thus being especially suited for applications in fixed bed and Berty reactors.

While information on the kinetics of the homogeneous, platinum catalyzed hydrogenation of diketones is well known[9] there is scarce information on the kinetics of the heterogeneous hydrogenation of α,β-diketones to α-hydroxy-carbonyl compounds and α,β-diols. In this work the liquid phase hydrogenation of

* *Correspondence to: Carlos R. Vera, INCAPE, Santiago del Estero 2654, 3000 Santa Fe, Argentina. E-mail: cvera@fiq.unl.edu.ar*

a *INCAPE-CONICET, Instituto de Investigaciones en Catálisis y Petroquímica, Santiago del Estero 2654, S3000AOJ Santa Fe, Argentina*

b *Facultad de Ingeniería Química (UNL), Santiago del Estero 2829, S3000AOJ Santa Fe, Argentina*

2,3-butanedione to 3-hydroxy-2-butanone has been carried out over composite supported palladium catalysts. Values of conversion to different products as a function of time, temperature, pressure and reactant concentration were used to assess different kinetic models. The models were developed by means of the Langmuir–Hinshelwood–Hougen–Watson (LHHW) methodology and kinetic and adsorption parameters were estimated by regressing experimental data. While the tested models gave insight into the underlying reaction mechanism, the quantitative information on reaction rate parameters is deemed useful for the simulation and optimization of industrial reactors.

EXPERIMENTAL

Support preparation

The reagents used in the composite support preparation were the following: (1) monomers: triethylene glycol dimethacrylate (TEGDMA, Aldrich Cat. N° 261548, CAS:109-16-0) and bisphenol A glycerolate dimethacrylate (BisGMA Aldrich Cat. N° 494356, CAS: 1565-94-2); (2) polymerization initiator: benzoyl peroxide (BPO Aldrich Cat. N° 179981, CAS: 94-36-0); (3) inorganic phase: γ-Al_2O_3 crushed to an average particle size of 0.074 mm (mesh 200).

The composite support was prepared using an equimolar mixture of the TEGDMA and BisGMA monomers and an appropriate quantity of BPO and γ-Al_2O_3. Details on the preparation procedure can be found elsewhere.[8] The support pellets were obtained by extrusion and had 3 mm length and 1.2 mm diameter. The pelletized composite support thus prepared was called BTAl.

Catalyst preparation

A supported Pd catalyst was prepared by means of incipient wetness impregnation of the BTAl support with an aqueous acidic solution of $PdCl_2$ (Fluka, Cat No: 76050, purity >99.98%) at a pH of 1. The Pd concentration in the solution was adjusted in order to obtain *c.* 0.3 wt% of Pd in the final catalyst. The catalyst was then dried in an oven at 393 K for 24 h and put in a desiccator for further use. This catalyst sample was named 0.3PdBTAl.

Two different portions of the catalyst were used. One was used for the reaction in the pellet form to check the activity and selectivity in the hydrogenation of 2,3-butanedione to 3-hydroxy-2-butanone. The other portion was milled to a powder and used in the kinetic studies. The small particle size of the powder ensured the absence of internal and external mass transfer resistances. The appropriate particle size to guarantee chemical control in the hydrogenation reaction was determined experimentally.

Characterization tests

The bulk Pd composition of the 0.3PdBTAl catalyst was obtained by digesting the sample with aqua regia and analyzing the liquors in a Perkin Elmer Optima 2100DV ICP equipment. X-ray diffractograms (XRD) were obtained in a Shimadzu XD-1 equipment, using CuKα radiation filtered with Ni and a scan speed of 2° min^{-1}. Scanning electron microscopy (SEM) was performed using a JEOL JSM-35C unit equipped with an energy dispersion system (EDAX). Micrographs were obtained with a Mitsubishi Microwatcher VS-30H Microscope and a Sony Color Video Printer. X-ray photoelectron spectroscopy (XPS) measurements were carried out with a Multitech UniSpecs equipment. The metal penetration in the support particles was determined by Electron Probe Microanalysis (EPMA). Values of the Pd/Al mass ratio inside the catalyst pellets were thus obtained as a function of the particle radius. Before the microscopy measurements the catalyst pellets were coated with a layer of carbon by vacuum deposition. The scanning speed of the probe was 0.02 mm min^{-1} and the acceleration voltage of the electron beam was 20 kV.

Values of the radial and axial mechanical resistance of the BTAl and γ-Al_2O_3 supports were obtained with an Instron Marks Universal Rehearsals equipment. A compression rate of 1 mm min^{-1} was used.

Catalytic tests

The liquid phase hydrogenation of 2,3-butanedione using powdery or pelletized catalysts was carried out in a semi-continuous PTFE-coated stainless steel tank reactor of 40 mL volume with mechanical stirrer. The tests with the pelletized catalysts were performed using a Berty reactor type[10] while for the kinetic studies with the powdery catalyst a slurry reactor was used.

Before starting the reaction test the catalyst was activated in hydrogen (50 mL h^{-1}, 503 K, 1 h). The reaction conditions were varied as follows: initial concentration of 2,3-butanedione = 0.19–0.72 mol L^{-1}, temperature = 313–353 K, total pressure = 10–40 bar.

A certain volume of a solution of 2,3-butanedione (Aldrich, Cat. N° B85307, purity 97%) dissolved in isopropyl alcohol (Cicarelli, purity 99%) and 1 g of the 0.3PdBTAl catalyst were charged to the reactor under nitrogen blanketing. The nitrogen pressure was then raised to 2 bar, the reactor stirrer was started and the system was heated to the desired reaction temperature. Then the reactor was flushed with hydrogen and pressurized to the desired value. This was considered the start time of the reaction. The tests were carried out in triplicate to decrease the experimental error. The overall repeatability was found to be within 3% error.

The reaction products mixture was analyzed by ex-situ gas chromatography using a Shimadzu GC-2010 equipped with a flame ionization detector and a 30 m J&W INNOWax 19091N-213 (cross-linked polyethylene glycol phase) capillary column.

Kinetic regime verification

The stirring rate and the catalyst particle size were varied in order to determine the values that ensured the absence of extra and intra-particle mass transfer limitations.[11] It was found that the reaction rate became practically constant for catalyst particle sizes lower than 10 μm and stirring rates higher than 1000 rpm. The absence of internal and external mass transfer limitations was also verified by using the Weisz-Prater and Mears criteria.[12]

Kinetic modeling

The reaction network of possible transformation pathways at the reaction conditions employed in this work is that described in Fig. 1. A first step of hydrogenation of one carbonyl of 2,3-butanedione (*DC*) leads to the formation of acetoin (*AC*). A further hydrogenation of the second carbonyl would lead to the formation of α,β-butanediol (*BD*). The occurrence of hydrogenolysis of the carbonyl group to a methylene group was not possible at the reaction conditions used and for this reason this is not considered in the reaction scheme of Fig. 1.

Only negligible amounts of 2,3-butanedione were detected among the reaction products. Due to the high selectivity of the Pd catalyst only the one-carbonyl selective hydrogenation to acetoin was considered in the kinetic study. The global reaction was further decomposed into elementary steps comprising the adsorption of 2,3-butanedione, the adsorption of hydrogen, the surface reaction of carbonyl hydrogenation and the desorption of products.

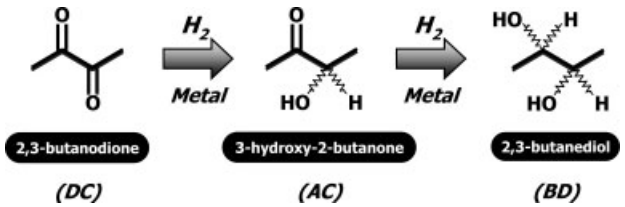

Figure 1. Reaction network for 2,3-butanedione hydrogenation over metal catalysts.

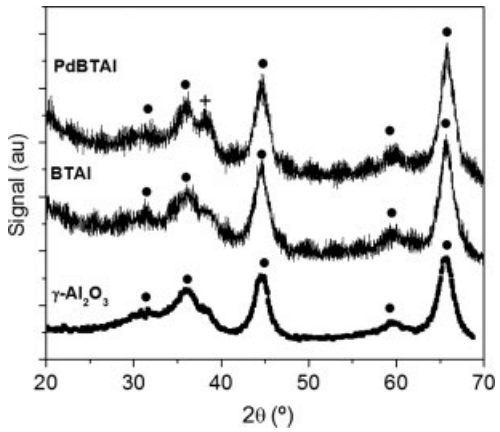

Figure 2. X-ray diffractograms of the supports and the Pd catalyst: (●) γAl_2O_3; (✙) Pd.

RESULTS

Catalyst characterization

The Pd content of the 0.3PdBTAl catalyst as determined by ICP was 0.26 wt%. X-ray diffractograms of the 0.3PdBTAl, BTAl and γ-Al_2O_3 samples are shown in Fig. 2. A high intensity peak at 39.9° corresponding to the (111) plane of metallic Pd can be seen in the spectrum of the 0.3PdBTAl catalyst. Low intensity peaks corresponding to other Pd reflection planes overlap with the characteristic signals of the γ phase of Al_2O_3. It is important to note that the diffractogram of the composite supported catalyst only shows peaks corresponding to γ-Al_2O_3 and Pd, and no signals due to the polymeric matrix. This is consistent with the bulk radical reaction procedure used that produces a completely amorphous polymeric phase.

SEM micrographs of the 0.3PdBTAl catalyst obtained with different levels of lens zoom are included in Fig. 3. In these images the location of Pd on the external surface of the support can be clearly appreciated. In the magnified images of Fig. 3(c) the three phases of the composite catalyst, alumina, polymer and palladium, can be clearly distinguished.

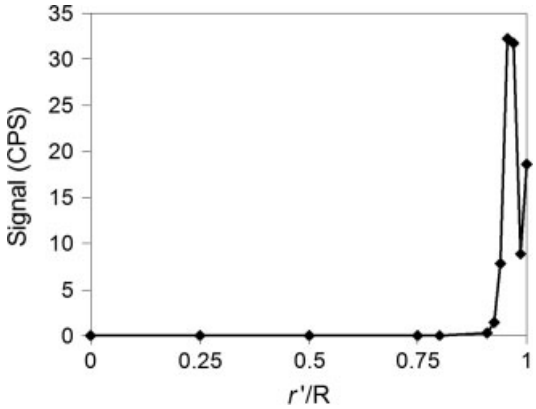

Figure 4. Metallic radial penetration profile of the 0.3PdBTAl catalyst as obtained by EPMA.

Figure 3(b) is a magnification of the outer surface of the composite, indicating the presence of Pd particles, as confirmed by EPMA. The average thickness of the egg-shell zone for the 0.3PdBTAl catalyst sample, as determined by EPMA, was approximately 90 µm. The metal radial penetration profile of the 0.3PdBTAl catalyst, also determined by EPMA, is shown in Fig. 4. A slight increase in Pd concentration at 20–30 µm from the border can be seen, thus confirming the existence of an egg-shell structure.

The Pd $3d_{5/2}$ XPS spectrum of the 0.3PdBTAl catalyst, previously reduced in H_2 at 503 K, is shown in Fig. 5. The spectrum presented a peak at about 198.5 eV that corresponds to Cl $2p_{3/2}$ associated to chloride species that were not eliminated during the thermal treatment.[13] A Cl/Pd atomic ratio equal to 0.84 (at/at) indicates that a high content of Cl is still present on the surface of the catalyst after its reduction. In Fig. 5 the typical $3d_{5/2}$ signals of metallic palladium can be found at binding energy (BE) peak values of: 335.6 eV (75.6 % at/at) and 336.6 eV (24.4 % at/at), with their corresponding Pd $3d_{3/2}$ doublets at 340.8 eV and 341.8 eV, respectively, attributed to the presence of $Pd^{\delta+}$ (with δ close to 0) and electrodeficient Pd^{n+} (with n close to 2) that appear by interaction of the Pd particles with surface oxychloride species of neighbouring Cl atoms.[14–16]

Values of the resistance to radial (DR) and axial compression (LR) of the BTAl support are included in Table 1. Values for α-Al_2O_3 and γ-Al_2O_3 are also included for the sake of comparison. It can be seen that the BTAl support has higher mechanical resistance than any of the reference materials. In this sense BTAl is a convenient support for preparing hydrogenation catalysts to be used in applications with high compression and attrition stress, such as packed beds, slurry and moving bed reactors.

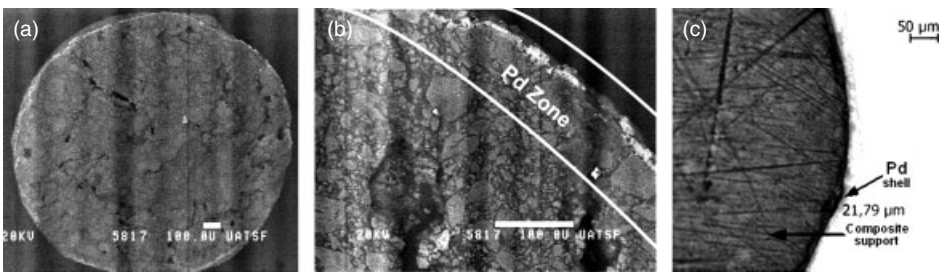

Figure 3. SEM micrographs of the cross-section of a 0.3PdBTAl catalyst pellet.

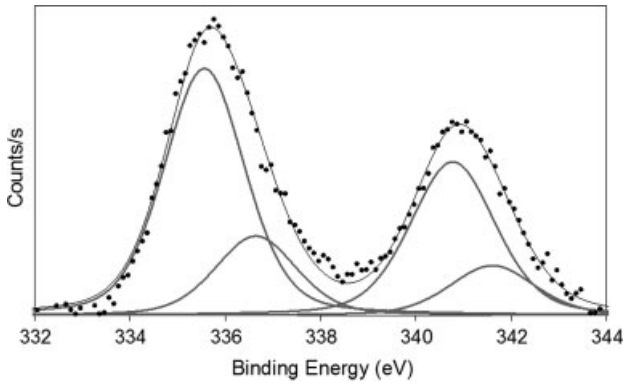

Figure 5. XPS spectrum of the 0.3PdBTAl catalyst, after being reduced in H_2 at 503 K.

Table 1. Mechanical properties of the supports. Diametral (DR) and longitudinal (LR) resistance to compression

	DR (kg cm^{-2})	LR (kg cm^{-2})
γ-Al_2O_3	< 100	703 ± 199
BTAl	392 ± 57	4708 ± 690
α-Al_2O_3	282 ± 43	2053 ± 398

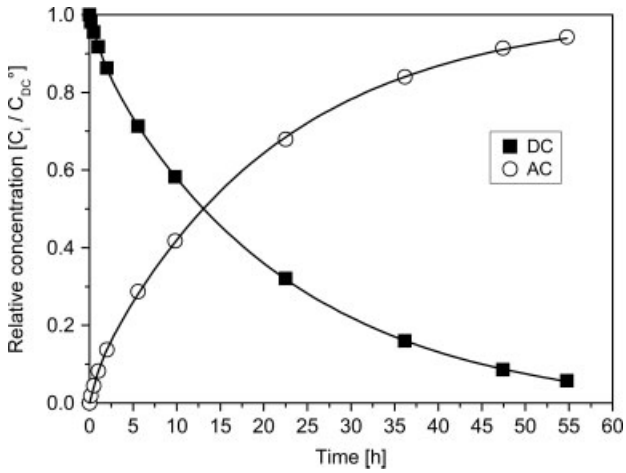

Figure 6. Relative concentration of 2,3-butanodione as a function of time-on-stream. Pelletized catalyst ($C_{DC}^{\circ} = 0.37$ mol L^{-1}, T = 343 K, $P = 40$ bar, $n = 1200$ rpm).

Butanedione hydrogenation results

Prior to the kinetic study some tests with the catalysts in the form of pellets were performed in order to make a screening of the best reaction conditions. Activity and selectivity in the hydrogenation of 2,3-butanedione (*DC*) to 3-hydroxy-2-butanone (*AC*) over 0.3PdBTAl were thus obtained. The results of a long-term reaction test are included in Fig. 6. The results indicate that the catalyst has high selectivity to the intermediate product of partial hydrogenation (α-hydroxy-ketone, *AC*). Only negligible traces of the product of hydrogenation of both carbonyls, 2,3-butanediol, could be detected even after 55 h of reaction time.

As calculated from the slope of the conversion–time plot, the initial reaction rate in the test with pelletized catalyst was 20 mmol h^{-1} L^{-1}, a moderate value that ensures the absence of mass diffusion constraints.

The results of tests with the catalyst in powder form are included in Fig. 7. Only values of conversion are plotted since the selectivity to *AC* was higher than 99% in all test runs and at all values of the reaction time. The effect of the hydrogen partial pressure is depicted in Fig. 7(a). The values of total system pressure were 10, 20, 30 or 40 bar, keeping all other variables constant (343 K, C^0_{DC}=0.37 mol L^{-1}). The hydrogen partial pressure was calculated considering that the partial pressures of *AC* and *DC* were equal to their vapor pressures, which were estimated by Antoine's equation. The parameters of this equation were taken from the NIST database.[17]

The plots of conversion of butanedione (X_{DC}) as a function of time in Fig. 7(a) indicate that the reaction rate increases when the partial pressure of hydrogen increases. The local slope of the curve yields the rate of conversion of *DC* for any value of reaction time. Values of the initial *DC* conversion rate per unit of catalyst mass (r^0_{DC}, mol$_{DC}$ h^{-1} g^{-1}) were calculated by polynomial differentiation of the curves at zero time. The reaction order with respect to hydrogen was calculated by considering that r^0_{DC} could be described by a power-law equation:

$$r^0_{DC} = k \cdot (p_{H2})^{\alpha} \cdot \left(C^0_{DC}\right)^{\beta} \quad (1)$$

The hydrogen reaction order (α), as determined by both linear and non-linear regression of Equation (1), was 0.48. This is almost equal to 0.5 (see Fig. 8(a)), the final value adopted for α.

The effect of the initial concentration of *DC* on the catalytic activity was studied at 343 K and p_{H2}=19.4 bar. The initial concentration of *DC* was varied between 0.19 and 0.72 mol L^{-1}. The results are shown in Fig. 7(b) and indicate that the catalyst activity decreases when the initial *DC* concentration is increased. The reaction order with respect to *DC* (β) was determined by calculating r^0_{DC} from the data of Fig. 7(b) and applying both linear and non-linear regression of these data with Equation (1). The fitted value was negative, β=−0.27 (see Fig. 8(b)).

The influence of the reaction temperature on the catalytic activity was studied in the 313–353 K range, at p_{H2}=19.4 bar and C^0_{DC}=0.37 mol L^{-1}. As expected Fig. 7(c) shows that the reaction rate was increased at higher temperatures. The apparent activation energy (E_A) was determined by fitting an Arrhenius-type relation and a value of E_A=33.1 kJ mol^{-1} was obtained (Fig. 8(c)).

The fact that the *DC* hydrogenation tests with the 0.3PdBTAl catalyst yielded a negative reaction order with respect to *DC* indicates that the interaction of *DC* with the surface active sites of this catalyst is very strong. In contrast, the positive order with respect to hydrogen indicates that at the working conditions the interaction of hydrogen is not so strong and is enhanced by an increase in pressure.

In order to explain the activity pattern in detail, especially with regards to the hydrogen pressure and *DC* concentration, kinetic models were developed. They are presented in the next section.

Kinetic modeling. LHHW models

Based on the previously discussed results Langmuir–Hinshelwood–Hougen–Watson models were developed. The following assumptions were made:

i Only one reaction mechanism is acting over the whole range of conditions used.
ii The adsorption of *DC* and the adsorption of H_2 are competitive (models with only one active site).

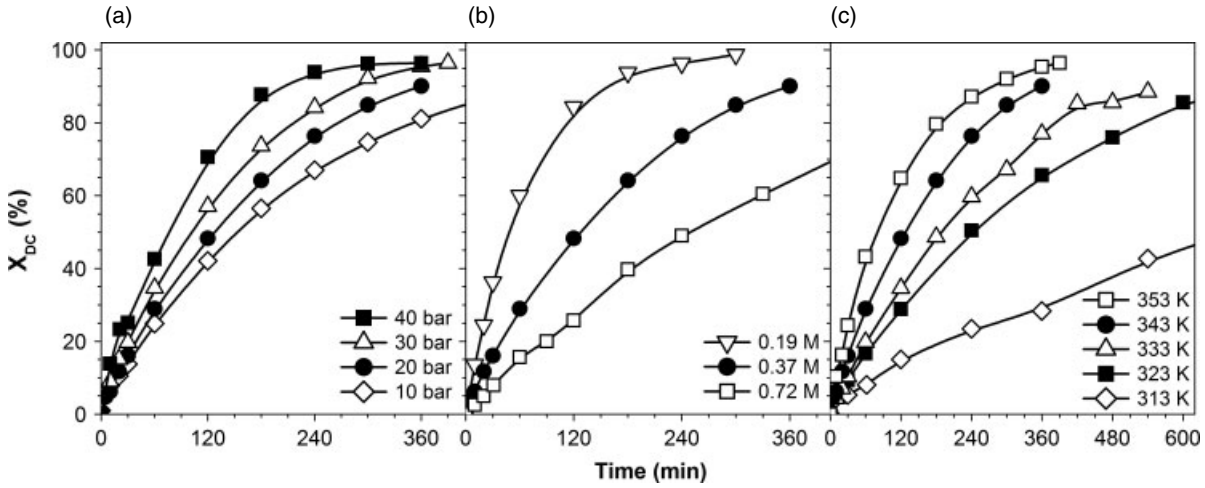

Figure 7. 2,3-butanodione conversion as a function of the reaction time (W_{CAT}=1 g, V_{SOLV}= 30 mL 2-propanol). (a) Influence of total pressure (T=343 K, C^0_{DC}=0.37 mol L^{-1}). (b) Influence of *DC* initial concentration (T= 343 K, p_{H2}= 19.4 bar). (c) Influence of temperature (p_{H2}= 19.4 bar, C^0_{DC}= 0.37 mol L^{-1}).

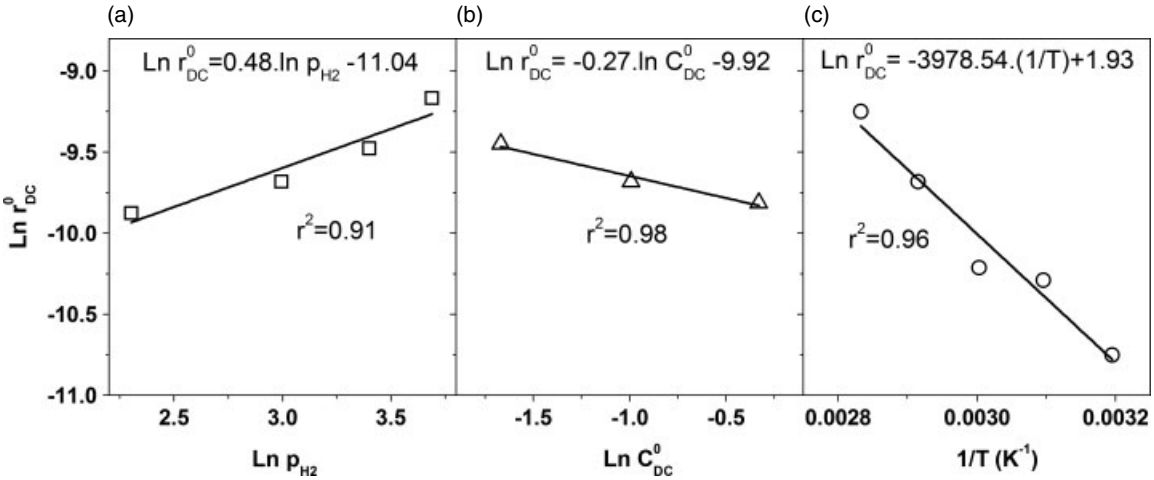

Figure 8. Values of the initial reaction rate as a function of: (a) hydrogen pressure (T= 343 K, C^0_{DC}=0.37 mol L^{-1}); (b) *DC* initial concentration (T=343 K, p_{H2}=19.4 bar); (c) temperature (p_{H2}=19.4 bar, C^0_{DC}=0.37 mol L^{-1}).

iii The adsorption of hydrogen can either be dissociative[18] or non-dissociative.[19]
iv If hydrogen reacts in the atomic state the addition of hydrogen to the *DC* molecule occurs in two steps (as in the Horiuti–Polanyi mechanism).
v The liquid phase is saturated in hydrogen throughout the test reaction time, the saturation value being given by Henry's law. This is assumed on the basis of the high stirring rate, the high dilution of the reactant in the liquid phase and the constant high hydrogen pressure.
vi *AC* adsorption and desorption are reversible quasi-equilibrium steps.
vii The adsorption of the reaction solvent, isopropyl alcohol, is considered to be negligible.
viii The hydrogenation reaction is irreversible (total conversion of *DC* into *AC* was observed in all the experiments).
ix The desorption of the first hydrogenation product, *AC*, is not a rate-limiting step.

Considering the former set of hypotheses, the elementary steps depicted in Equations (2)–(5) represent the general reaction mechanism (S=active site):

Butanedione adsorption:

$$DC + S \Leftrightarrow DC - S \quad r_1 = k_{DC} \cdot C_{DC} \cdot C_S - k^{-1}_{DC} \cdot C_{DC-S} \tag{2}$$

Hydrogen dissociative chemisorption:

$$H_2 + 2\,S \Leftrightarrow 2\,H - S \quad r_2 = k_{H2} \cdot p_{H2} \cdot (C_S)^2 - k^{-1}_{H2} \cdot (C_{H-S})^2 \tag{3}$$

Hydrogen non-dissociative chemisorption:

$$H_2 + S \Leftrightarrow H_2 - S \quad r_3 = k_{H2} \cdot p_{H2} \cdot C_S - k^{-1}_{H2} \cdot C_{H2-S} \tag{4}$$

Surface single-step hydrogenation reaction:

$$2\,H - S + DC - S \Leftrightarrow AC - S + 2\,S \quad r_4 = k_{SR} \cdot (C_{H-S})^2 \cdot C_{DC-S} \tag{5}$$

$$H_2 - S + DC - S \Leftrightarrow AC - S + S \quad r_5 = k_{SR} \cdot C_{H2-S} \cdot C_{DC-S} \tag{6}$$

Surface two-step hydrogenation reaction (Horiuti-Polanyi):

$$H - S + DC - S \Rightarrow DCH - S + S \quad r_6 = k_{SR1} \cdot C_{H-S} \cdot C_{DC-S} \tag{7}$$

$$H - S + DCH - S \Rightarrow AC - S + S \quad r_7 = k_{SR2} \cdot C_{H-S} \cdot C_{DCH-S} \tag{8}$$

Acetoin desorption:

$$AC - S \Leftrightarrow AC + S \quad r_8 = k_{AC}^{-1} \cdot C_{AC-S} - k_{AC} \cdot C_{AC} \cdot C_S \tag{9}$$

For a discontinuous closed system with no spatial gradients (perfectly mixed reactor) the differential mass balance for the *AC* and *DC* compounds can be written as:

$$\frac{dC_{DC}^*}{dt} = \frac{1}{C_{DC}^0} \cdot \frac{dC_{DC}}{dt} = -\frac{1}{C_{DC}^0} \cdot r \tag{10}$$

$$\frac{dC_{AC}^*}{dt} = \frac{1}{C_{DC}^0} \cdot \frac{dC_{AC}}{dt} = \frac{1}{C_{DC}^0} \cdot r \tag{11}$$

where r is the rate of the limiting step in the reaction mechanism and $C_i^* = C_i/C_{DC}^0$ the relative concentration of the i component. The working reaction mechanism is a subset of the steps (2)–(7).

By assuming different rate-limiting steps (r.l.s.) (adsorption of H_2, adsorption of *DC* or surface chemical reaction), and two possible ways of hydrogen chemisorption (dissociative and non-dissociative) 14 different LHHW models can be generated. Details of these models are given in Table 2. The expressions obtained for the final reaction rate r in Table 2 were simplified by renaming groups of kinetic and equilibrium constants as P_j parameters.

Models 1 to 12 in Table 2 assume hydrogenation to proceed by surface reaction in the adsorbed state and in only one step, i.e. by addition of molecular hydrogen or by pairwise addition of two hydrogen atoms. Models 13 and 14 are the combination of steps (2), (3), (7) and (8) and involve the sequential addition of one hydrogen atom at a time. This is the sequence of the Horiuti–Polanyi hydrogenation mechanism.[20,21] This mechanism has been proved to be the working one in the metal catalyzed hydrogenation of olefins. The Horiuti–Polanyi mechanism assumes that one of the two surface-reaction steps is rate-limiting and that the other one is in equilibrium.

Hydrogenation of aldehydes and ketones resembles the hydrogenation of olefins to alkanes in that two hydrogen atoms are added across a C=O or C=C double bond. In this sense, the extension of the Horiuti–Polanyi mechanism to the carbonyl hydrogenation has raised concerns owing to: (i) the existence of two different 'half-hydrogenated states'; (ii) the polar nature of the carbonyl double bond; (iii) the existence of lone pair oxygen electrons; (iv) the lower irreversibility of the reaction. A comprehensive review on the catalytic hydrogenation of aldehydes and ketones in the liquid phase was written by Cerveny.[22] On the basis of numerous deuterium tracer studies the author concludes that the Horiuti–Polanyi partial hydrogenation mechanism can be extended to ketone hydrogenation on most noble metals, though the nature of the adsorbed bond is reported to be different from that found in the olefin–metal system. According to spectral evidence the molecular species in the adsorbed state would be either π-bonded or coordinated through the oxygen lone pairs. The occurrence of an alkoxy intermediate (Fig. 9, reaction pathway 'a') or a hydroxyalkyl intermediate (Fig. 9, reaction pathway 'b') is a matter of debate and is strongly dependent on the reacting system. Early work on vapor phase hydrogenation indicated that the intermediate product of half-hydrogenation was CH–O* (alkoxy) rather than C*–OH (hydroxyalkyl) (Fig. 9) because OH vibrations could not be detected in spectroscopy studies.[24] However, in the case of carbonyl hydrogenations in the liquid phase, intermediate hydroxyalkyl species have been reported to be stabilized by protic solvents such as water and methanol.[25]

The equation of Model 13 has been derived from the general hypotheses (i)–(ix) listed above and the mechanistic sequence (2)–(3)–(7)–(8). The adopted rate-limiting step is (7) and step (8) has been considered to be an irreversible equilibrium so that the surface concentration of the half-hydrogenation product is negligible. A similar model has been proposed for the liquid-phase hydrogenation of citronellol over Raney Ni catalysts.[26] Considering step (8) as rate-limiting leads to the equation of Model 14. In deriving such equation the surface concentration of the half-hydrogenated intermediate has again been considered negligible.

Kinetic modeling. Numerical resolution and statistics

The system of differential equations (Equations (10) and (11)) was solved numerically using the Runge–Kutta–Merson algorithm. The model parameter estimation was performed by nonlinear regression using a Levenberg–Marquardt algorithm that minimized an objective function based on the sum of the squares of the deviations:

$$S = \sum_t \left(C_{i,t}^* - C_{i,t}^{*CALC}\right)^2 \tag{12}$$

where $C_{i,t}^*$ and $C_{i,t}^{*CALC}$ are the experimental and calculated concentrations, respectively. i is the chemical compound index, and t is the reaction time.

The coefficient of determination (*CoD* or r^2) gave the fitting quality (i.e. the percentage of explanation of the total data variation around the average observed value) and was calculated using Equation (13).

$$CoD = r^2 = \frac{\sum_{i=1}^{n} \left(C_i^{*CALC} - \overline{C^*}\right)^2}{\sum_{i=1}^{n} \left(C_i^* - \overline{C^*}\right)^2} \tag{13}$$

The model adequacy and the discrimination between models were determined using the model selection criterion (MSC), according to the following equation:

$$MSC = \ln\left[\frac{\sum_{i=1}^{n} \left(C_i^* - \overline{C^*}\right)^2}{\sum_{i=1}^{n} \left(C_i^* - C_i^{*CALC}\right)^2}\right] - \left(\frac{2 \cdot p}{n}\right) \tag{14}$$

where n is the number of experimental data, p is the amount of parameters fitted, $\overline{C^*}$ is the average relative concentration and $C_{i,t}^{*CALC}$ and $C_{i,t}^*$ are the predicted and experimental values, respectively. When various different models are compared the most significant one is that with the highest *MSC* value.

Kinetic modeling results

The mathematical expressions of the overall rate of conversion of *DC* as obtained with the different models are listed in Table 2. Models 1, 4, 7 and 10, that posed *DC* adsorption as rate-limiting, yield reaction rate formulae that cannot provide a negative

Table 2. LHHW kinetic models assuming the surface reaction as the rate-limiting step. Full expressions and simplified ones with minimum number of parameters. *SSD*: sum of squared deviations; *CoD*: coefficient of determination; *MSC*: model selection criterion; r^*: reaction rate for negligible hydrogen surface coverage

Model	Reaction rate full and simplified equations	Fitting results
Model 1 Dissociative H_2 chemisorption Total coverage of sites r.l.s.: *DC* adsorption	$r = \frac{k_{DC} \cdot C_T \cdot C_{DC}}{(\sqrt{K_{H2} \cdot p_{H2}} + K_{AC} \cdot C_{AC})}$ $r = \frac{P_1 \cdot C_{DC}}{(\sqrt{p_{H2}} + P_2 \cdot C_{AC})}$	Cannot explain experimental apparent negative order in *DC*
Model 2 Dissociative H_2 chemisorption Total coverage of sites r.l.s.: H_2 adsorption	$r = \frac{k_{H2} \cdot p_{H2} \cdot (C_T)^2}{(K_{DC} \cdot C_{DC} + K_{AC} \cdot C_{AC})^2}$ $r = \frac{P_1 \cdot p_{H2}}{(C_{DC} + P_2 \cdot C_{AC})^2}$	Non-convergence error
Model 3 Dissociative H_2 chemisorption Total coverage of sites r.l.s.: surface chemical reaction	$r = \frac{k_{SR} \cdot K_{DC} \cdot K_{H2} \cdot p_{H2} \cdot (C_T)^3 \cdot C_{DC}}{(\sqrt{K_{H2} \cdot p_{H2}} + K_{DC} \cdot C_{DC} + K_{AC} \cdot C_{AC})^3}$ $r = \frac{P_1 \cdot p_{H2} \cdot C_{DC}}{(\sqrt{p_{H2}} + P_2 \cdot C_{DC} + P_3 \cdot C_{AC})^3}$	*SSD*=0.058 *CoD*=0.984 *MSC*=4.119 P_1=0.172 ± 0.032 P_2=8.892 ± 1.080 P_3=8.856 ± 1.600
	$r* = \frac{P_1^* \cdot p_{H2} \cdot C_{DC}}{(C_{DC} + P_3^* \cdot C_{AC})^3}$	*SSD**=0.420 *CoD**=0.887 *MSC**=2.157 $P_1{}^*$=6.8E-5 ± 2.6E-5 $P_3{}^*$=2.076 ± 0.506
Model 4 Dissociative H_2 chemisorption Partial coverage of sites r.l.s.: *DC* adsorption	$r = \frac{k_{DC} \cdot C_T \cdot C_{DC}}{(1 + \sqrt{K_{H2} \cdot p_{H2}} + K_{AC} \cdot C_{AC})}$ $r = \frac{P_1 \cdot C_{DC}}{(1 + P_2 \cdot \sqrt{p_{H2}} + P_3 \cdot C_{AC})}$	Cannot explain experimental positive order in hydrogen
Model 5 Dissociative H_2 chemisorption Partial coverage of sites r.l.s.: H_2 adsorption	$r = \frac{k_{H2} \cdot p_{H2} \cdot (C_T)^2}{(1 + K_{DC} \cdot C_{DC} + K_{AC} \cdot C_{AC})^2}$ $r = \frac{P_1 \cdot p_{H2}}{(1 + P_2 \cdot C_{DC} + P_3 \cdot C_{AC})^2}$	Non-convergence error
Model 6 Dissociative H_2 chemisorption Partial coverage of sites r.l.s.: surface chemical reaction	$r = \frac{k_{SR} \cdot K_{DC} \cdot K_{H2} \cdot p_{H2} \cdot (C_T)^3 \cdot C_{DC}}{(1 + \sqrt{K_{H2} \cdot p_{H2}} + K_{DC} \cdot C_{DC} + K_{AC} \cdot C_{AC})^3}$ $r = \frac{P_1 \cdot p_{H2} \cdot C_{DC}}{(1 + P_2 \cdot \sqrt{p_{H2}} + P_3 \cdot C_{DC} + P_4 \cdot C_{AC})^3}$	*SSD*=0.016 *CoD*=0.996 *MSC*=5.388 P_1=0.0075 ± 0.0024 P_2=0.194 ± 0.039 P_3=2.820 ± 0.357 P_4=2.125 ± 0.462
	$r* = \frac{P_1^* \cdot p_{H2} \cdot C_{DC}}{(1 + P_3^* \cdot C_{DC} + P_4^* \cdot C_{AC})^3}$	*SSD**=0.060 *CoD**=0.983 *MSC**=4.088 $P_1{}^*$=0.0012 ± 0.0002 $P_3{}^*$=1.493 ± 0.2023 $P_4{}^*$=1.221 ± 0.281
Model 7 Non-dissociative H_2 chemisorption Total coverage of sites r.l.s.: *DC* adsorption	$r = \frac{k_{DC} \cdot C_T \cdot C_{DC}}{(K_{H2} \cdot p_{H2} + K_{AC} \cdot C_{AC})}$ $r = \frac{P_1 \cdot C_{DC}}{(P_2 \cdot p_{H2} + P_3 \cdot C_{AC})}$	Cannot explain experimental apparent negative order in *DC*
Model 8 Non-dissociative H_2 chemisorption Total coverage of sites r.l.s.: H_2 adsorption	$r = \frac{k_{H2} \cdot p_{H2} \cdot C_T}{(K_{DC} \cdot C_{DC} + K_{AC} \cdot C_{AC})}$ $r = \frac{P_1 \cdot p_{H2}}{(C_{DC} + P_2 \cdot C_{AC})}$	Non-convergence error
Model 9 Non-dissociative H_2 chemisorption Total coverage of sites r.l.s.: surface chemical reaction	$r = \frac{k_{SR} \cdot K_{DC} \cdot K_{H2} \cdot p_{H2} \cdot (C_T)^2 \cdot C_{DC}}{(K_{H2} \cdot p_{H2} + K_{DC} \cdot C_{DC} + K_{AC} \cdot C_{AC})^2}$ $r = \frac{P_1 \cdot p_{H2} \cdot C_{DC}}{(p_{H2} + P_2 \cdot C_{DC} + P_3 \cdot C_{AC})^2}$	*SSD*=0.035 *CoD*=0.990 *MSC*=4.612 P_1=1.457 ± 0.279 P_2=110.136 ± 14.586 P_3=120.484 ± 19.305
	$r* = \frac{P_1^* \cdot p_{H2} \cdot C_{DC}}{(C_{DC} + P_3^* \cdot C_{AC})^2}$	*SSD**=0.154 *CoD**=0.958 *MSC**=3.159 $P_1{}^*$= 7.1E-5 ± 1.2E-5 $P_3{}^*$=1.328 ± 0.266
Model 10 Non-dissociative H_2 chemisorption Partial coverage of sites r.l.s.: *DC* adsorption	$r = \frac{k_{DC} \cdot C_T \cdot C_{DC}}{(1 + K_{H2} \cdot p_{H2} + K_{AC} \cdot C_{AC})}$ $r = \frac{P_1 \cdot C_{DC}}{(1 + P_2 \cdot p_{H2} + P_3 \cdot C_{AC})}$	Cannot explain experimental apparent negative order in *DC*
Model 11 Non-dissociative H_2 chemisorption Partial coverage of sites r.l.s.: H_2 adsorption	$r = \frac{k_{H2} \cdot p_{H2} \cdot C_T}{(1 + K_{DC} \cdot C_{DC} + K_{AC} \cdot C_{AC})}$ $r = \frac{P_1 \cdot p_{H2}}{(1 + P_2 \cdot C_{DC} + P_3 \cdot C_{AC})}$	Non-convergence error
Model 12 Non-dissociative H_2 chemisorption Partial coverage of sites r.l.s.: surface chemical reaction	$r = \frac{k_{SR} \cdot K_{DC} \cdot K_{H2} \cdot p_{H2} \cdot (C_T)^2 \cdot C_{DC}}{(1 + K_{H2} \cdot p_{H2} + K_{DC} \cdot C_{DC} + K_{AC} \cdot C_{AC})^2}$ $r = \frac{P_1 \cdot C_{DC} \cdot p_{H2}}{(1 + P_2 \cdot p_{H2} + P_3 \cdot C_{DC} + P_4 \cdot C_{AC})^2}$	*SSD*=0.018 *CoD*=0.995 *MSC*=5.297 P_1=0.0071 ± 0.0025 P_2=0.051 ± 0.014 P_3=7.517 ± 1.591 P_4=5.740 ± 1.457
	$r* = \frac{P_1^* \cdot C_{DC} \cdot p_{H2}}{(1 + P_3^* \cdot C_{DC} + P_4^* \cdot C_{AC})^2}$	*SSD**=0.059 *CoD**=0.984 *MSC**=4.101 $P_1{}^*$=0.0016 ± 0.0004 $P_3{}^*$=3.469± 0.6967 $P_4{}^*$=2.892 ± 0.824
Model 13 Dissociative H_2 chemisorption Partial coverage of sites Horiuti–Polanyi mechanism r.l.s.: formation of half-hydrogenation intermediate	$r = \frac{k_{SR1} \cdot K_{DC} \cdot \sqrt{K_{H2} \cdot p_{H2}} \cdot (C_T)^2 \cdot C_{DC}}{(1 + \sqrt{K_{H2} \cdot p_{H2}} + K_{DC} \cdot C_{DC} + K_{AC} \cdot C_{AC})^2}$ $r = \frac{P_1 \cdot \sqrt{p_{H2}} \cdot C_{DC}}{(1 + P_2 \cdot \sqrt{p_{H2}} + P_3 \cdot C_{DC} + P_4 \cdot C_{AC})^2}$	*SSD*=0.014 *CoD*=0.996 *MSC*=5.512 P_1=0.0065 ± 0.0013 P_2=0.0 ± 0.0205 P_3=3.287 ± 0.449 P_4=2.486 ± 0.383
	$r* = \frac{P_1^* \cdot \sqrt{p_{H2}} \cdot C_{DC}}{(1 + P_3^* \cdot C_{DC} + P_4^* \cdot C_{AC})^2}$	*SSD**=0.014 *CoD**=0.996 *MSC**=5.527 $P_1{}^*$= 0.0065 ± 0.0013 $P_3{}^*$=3.287 ± 0.449 $P_4{}^*$=2.486 ± 0.383
Model 14 Dissociative H_2 chemisorption Partial coverage of sites Horiuti–Polanyi mechanism r.l.s.: insertion of second hydrogen atom	$r = \frac{k_{SR2} \cdot K_{DC} \cdot K_{H2} \cdot K_{DCH} \cdot p_{H2} \cdot (C_T)^2 \cdot C_{DC}}{\left(1 + \sqrt{K_{H_2} \cdot p_{H_2}} + K_{DCH} \cdot K_{DC} \cdot C_{DC} \cdot \sqrt{K_{H_2} \cdot p_{H_2}} + K_{DC} \cdot C_{DC} + K_{AC} \cdot C_{AC}\right)^2}$ $r = \frac{P_1 \cdot p_{H2} \cdot C_{DC}}{\left(1 + P_2 \cdot \sqrt{p_{H_2}} + P_3 \cdot C_{DC} \cdot \sqrt{p_{H_2}} + P_4 \cdot C_{DC} + P_5 \cdot C_{AC}\right)^2}$	*SSD*=0.015 *CoD*=0.996 *MSC*=5.454 P_1=0.032 ± 0.115 P_2=0.801 ± 1.784 P_3=11.243 ± 27.555 P_4=11.943 ± 21.141 P_5=0.111 ± 0.517
	$r* = \frac{P_1^* \cdot p_{H2} \cdot C_{DC}}{(1 + P_4^* \cdot C_{DC} + P_5^* \cdot C_{AC})^2}$	*SSD**=0.059 *CoD**=0.984 *MSC**=4.101 $P_1{}^*$=0.0016 ± 0.0004 $P_4{}^*$=3.460 ± 0.697 $P_5{}^*$=2.882 ± 0.822

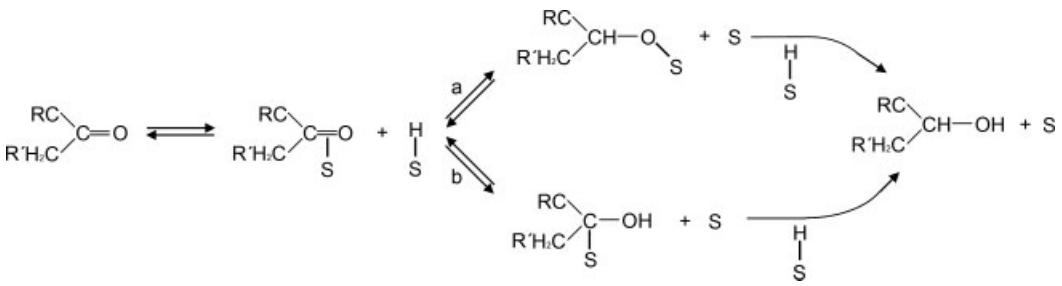

Figure 9. Horiuti–Polanyi polystep hydrogenation mechanism as applied to the hydrogenation of ketones (S is the active site). (a) alkoxy intermediate (b) hydroxyalkyl intermediate; taken from Tanaka.[23]

order with respect to C_{DC} or a positive order with respect to p_{H2} and should therefore be disregarded. Running the fitting procedure with these models only gave anomalous results or non-convergence problems.

An inspection of the results on the last column of Table 2 reveals that models 2, 5, 8 and 11, that posed hydrogen adsorption as rate-limiting, consistently had non-convergence problems. Only models 3, 6, 9, 12, 13 and 14, that posed the surface reaction as the rate limiting step, gave good fits of the experimental data.

The results of the least squares minimization algorithm consistently gave values for the K_{H2} constant that made the term $\psi=(K_{H2}\,p_{H2})^{1/2}$ negligible in comparison with the other adsorption terms (see models 6, 12 and 13 in Table 2). ψ is the term related to the fraction of sites covered by hydrogen and is many times considered to be negligible, especially if the system is dominated by the adsorption of the organic molecules.[27] This is also a consequence of the low solubility of hydrogen in most liquids. In this sense a collection of the reported values of the solubility of hydrogen and Langmuir constant for the dissociative adsorption of hydrogen over palladium for different systems in liquid solution and at almost the same conditions of those employed in this work, are included in Table 3. It can be confirmed that the term ψ is lower than 1 thus indicating that the fractional coverage of palladium by hydrogen (θ_{SH}) is negligible in comparison with the fraction of free sites (θ_S) (see Equation (17)), even at high pressure conditions (40 atm).

$$\theta_{SH}=\frac{C_{SH}}{C_T}=\frac{\sqrt{K_{H2}\cdot p_{H2}}}{C_T}C_S=\psi\cdot\frac{C_S}{C_T} \tag{15}$$

$$\theta_S=\frac{C_S}{C_T} \tag{16}$$

$$\frac{\theta_{SH}}{\theta_S}=\psi \tag{17}$$

where C_S and C_T are the free active site concentration and the total active site concentration, respectively.

In light of these results the term ψ was dropped from some equations of the models, considering it was negligible in comparison with the other adsorption terms. The new equations for small hydrogen coverage and with the minimum number of meaningful parameters are included as r^* in Table 2. Their calculated sum of squared deviations is noted as *SSD**.

According to the model selection criterion (*MSC*), the ranking for goodness of fit is: model 13 (Horiuti–Polanyi, first hydrogen insertion as limiting step) > model 14 (Horiuti–Polanyi, second hydrogen insertion as limiting step) > model 6 (dissociative adsorption, partial coverage of sites) > model 12 (non-dissociative adsorption, partial coverage of sites) ≫ model 9 (non-dissociative adsorption, total coverage of sites) > model 3 (dissociative adsorption, total coverage of sites). The analysis of the values of the sum of squared deviations (*SSD*) and coefficient of determination (*CoD* or r^2) yields the same order for goodness of fit.

Models 6, 12, 13 and 14 considered only a partial coverage of the active sites and did not eliminate the fraction of free sites. For this reason they contain an additional parameter for estimation with respect to models 3 and 9. This extra parameter permits a better fit of the data that seems completely necessary because the system is not working in conditions of total surface coverage. For example, if we consider model 13 and its calculated parameters (P_1, P_2, P_3 and P_4), an estimation of the fraction of free sites at zero conversion and negligible hydrogen adsorption yields a value of about 0.3. The fraction of free sites is therefore not negligible and models 3 and 9 should be disregarded.

The three models considering dissociative adsorption of hydrogen (models 6, 13 and 14) produced a better fit of the data than model 12 that had non-dissociative hydrogen adsorption as one underlying assumption. Experimental data and quantum chemical simulations on the adsorption of hydrogen on palladium particles consistently support the fact that hydrogen is almost instantaneously dissociated after molecular adsorption on the surface. Mechanistically speaking the energy gain due to the first exothermal molecular adsorption helps hydrogen to overcome the energy barrier for breaking the H–H bond.[35] On the basis of these comments only models 6, 13 and 14 should be finally considered to be valid.

The correct choice seems to be that of model 13, which has a number of advantages: (i) it correlates the experimental data set better than other models; (ii) it has a small number of adjustable parameters (P_1, P_2, P_3, P_4); (iii) the regressed value of the P_2 parameter is negligible compared with P_3 and P_4, as should be the case for the adsorption constant of hydrogen when compared with that of butanedione and acetoin; (iv) it predicts a 0.5 order in hydrogen, the same value found in the experiments.

The good correlation of the experimental data with kinetic model 13.b (r^*) was valid at most reaction conditions. For example the results obtained for three initial *DC* concentrations gave values of *MSC* higher than 6 in all cases whereas the sums of squared deviations were in the order of 10^{-3}. Figure 10(a) shows a good agreement between the experimental data (symbols) and the predictions of model 13.b (full lines) when the relative concentrations of *DC* and *AC* are represented as functions of time. The distribution of residuals also followed an acceptable random trend when represented as a function of time (Fig. 10(b)). This is consistent with the hypotheses of random error, implicit in the nonlinear regression procedure used for parameter estimation, and gives additional support to the adequacy of the model.

Table 3. Values of the solubility of hydrogen (S_{H2}), the Langmuir adsorption constant (K_{H2}) and the hydrogen coverage related term, $\psi = (K_{H2}\, p_{H2})^{1/2}$, for the dissociative adsorption of hydrogen on palladium

Property	Value	Conditions	Reference
S_{H2}	0.122 mol L^{-1}	40 atm, 298 K, 1-propanol	28
S_{H2}	0.335 mol L^{-1}	40 atm, 333 K, 1-propanol	29
S_{H2}	0.278 mol L^{-1}	42 atm, 353 K, 1-propanol	30
S_{H2}	0.081 mol L^{-1}	34 atm, 348 K, methanol	31
K_{H2}	8.72E-6 atm^{-1}	40 atm, 333 K, n-heptane	32
K_{H2}	4.25E-5 atm^{-1}	40 atm, 333 K, n-heptane	29,33
K_{H2}	5.00E-3 atm^{-1}	8 atm, 348 K, unsaturated alcohol	34
Ψ	0.018	40 atm, 333 K, n-heptane	32
Ψ	0.041	40 atm, 333 K, n-heptane	29,33
Ψ	0.200	8 atm, 348 K, unsaturated alcohol	34

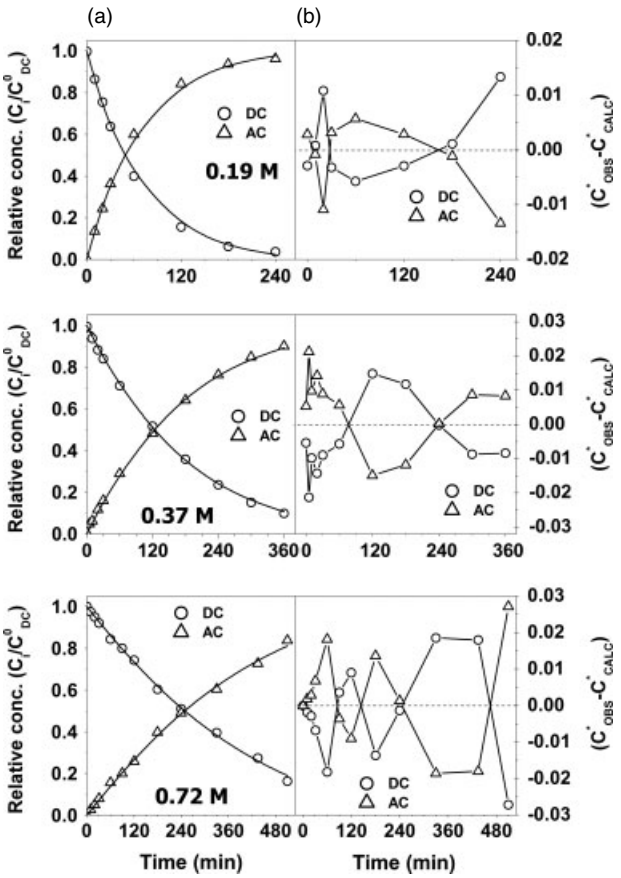

Figure 10. Comparison of the experimental results and theoretical predictions for the 2,3-butanedione hydrogenation over 0.3PdBTAl. (a) Experimental (symbols) and model results (full lines) for the LHHW Model 13.b. (b) Evolution of residuals for *DC* and *AC* (p_{H2}= 19.3 bar, W_{CAT}= 1 g, C^0_{DC}= 0.18 mol L^{-1}–0.72 mol L^{-1}, V_{SOLV}= 30 mL).

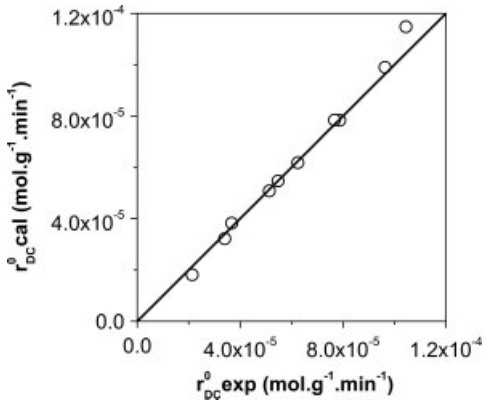

Figure 11. Parity plot of the experimental (exp) and calculated (cal) r^0_{DC} values for all the experimental conditions used.

Figure 11 is a parity plot showing the predicted initial reaction rates against the experimental values. The trend of the curve indicates that an excellent fit was achieved with Model 13.b.

When writing the P_j^* parameters of the reaction rate r^* in the corresponding Arrhenius and van't Hoff forms for the reaction and adsorption constants, the expressions written down in Table 4 are found. Grouping constants together enables one to obtain a minimum number of parameters while regression of the data permits one to obtain their numerical value. The regressed value of the activation energy for the surface reaction step is about 27 kCal mol^{-1}, while the heats of adsorption of butanedione and acetoin are about −3.2 and −4.6 kCal mol^{-1}, respectively. For estimation of the activation energy of the hydrogenation step, the heat of adsorption of hydrogen on palladium had to be taken into account. The value taken from a scientific literature reference[36] was −26 kCal mol^{-1}. The net effect of the exothermal heats of adsorption of the various species is to reduce the average energy barrier of the global reaction rate, indicated in Table 4 as E_1 and equal to 11 kCal mol^{-1}.

DISCUSSION

The characterization tests show that the 0.3PdBTAl catalyst has a good mechanical resistance, an egg-shell distribution of metal palladium particles and mainly one kind of active metal site (oxychlorided $Pd^{\delta+}$, with δ close to 0). The models developed for the catalytic hydrogenation of butanedione on this catalyst thus considered the competition of reagents and products for mainly one kind of site.

The best LHHW model to interpret the *DC* hydrogenation results on the 0.3PdBTAl catalyst (model 13.b, $r*$) considers that the adsorption of *DC* and H_2 on the palladium sites is competitive and that the rate-limiting step is the surface chemical reaction of addition of the first H atom (Horiuti–Polanyi mechanism). Furthermore, the model assumes dissociative adsorption of hydrogen, low hydrogen coverage, negligible adsorption of the half-hydrogenation reaction intermediate, strong adsorption of

Table 4. Values of the parameters of the Arrhenius and van't Hoff formulae for the P_1, P_2 and P_3 factors of the global chemical reaction rate equation, as described by the Horiuti–Polanyi model (see model 13 in Table 2, with negligible hydrogen adsorption). Values regressed from a set including data of reactions at 313, 323, 333 and 343 K

Property	Value and units
$r = \frac{k_{SR1}\cdot K_{DC}\cdot\sqrt{K_{H2}\cdot p_{H2}}\cdot(C_T)^2\cdot C_{DC}}{\left(1+\sqrt{K_{H2}\cdot p_{H2}}+K_{DC}\cdot C_{DC}+K_{AC}\cdot C_{AC}\right)^2}$ $r* = \frac{k_{SR1}\cdot K_{DC}\cdot\sqrt{K_{H2}\cdot p_{H2}}\cdot(C_T)^2\cdot C_{DC}}{(1+K_{DC}\cdot C_{DC}+K_{AC}\cdot C_{AC})^2}$ $r* = \frac{a_{SR1}\cdot e^{\frac{-E_A}{RT}}\cdot a_{DC}\cdot e^{\frac{-\Delta H_{DC}}{RT}}\cdot\sqrt{a_{H2}}\cdot e^{\frac{-\Delta H_{H2}}{2RT}}\sqrt{p_{H2}}\cdot(C_T)^2\cdot C_{DC}}{\left(1+a_{DC}\cdot e^{\frac{-\Delta H_{DC}}{RT}}\cdot C_{DC}+a_{AC}\cdot e^{\frac{-\Delta H_{AC}}{RT}}\cdot C_{AC}\right)^2}$ $r* = \frac{p_1\cdot e^{\frac{-(E_1)}{RT}}\cdot\sqrt{p_{H2}}\cdot C_{DC}}{\left(1+p_3\cdot e^{\frac{-\Delta H_{DC}}{RT}}\cdot C_{DC}+p_4\cdot e^{\frac{-\Delta H_{AC}}{RT}}\cdot C_{AC}\right)^2}$ $\left(E_1 = E_A + \Delta H_{DC} + \frac{\Delta H_{H2}}{2}\right)$	mol g^{-1} h^{-1}
$p_1 = a_{SR1}\cdot a_{DC}\cdot\sqrt{a_{H2}}\cdot(C_T)^2$	780 L $atm^{-1/2}$ g^{-1} h^{-1}
$p_3 = a_{DC}$	0.03703 L mol^{-1}
$p_4 = a_{AC}$	0.00406 L mol^{-1}
E_1	10.95 kCal mol^{-1}
ΔH_{DC}	−3.19 kCal mol^{-1}
ΔH_{AC}	−4.55 kCal mol^{-1}
ΔH_{H2} (Ref. 36)	−26 kCal mol^{-1}
Estimated E_A	27.14 kCal mol^{-1}

DC and *AC* on the metal sites and partial coverage of all active sites.

The strong adsorption of 2,3-butanedione over the Pd particles can be easily explained on the basis of the strength of the chelating metal–dicarbonyl bond, which is the basis for the stability of many metal–carbonyl complexes. Metal–carbon bonds in metal–carbonyl complexes have both π and σ character. The σ bond is formed when the carbonyl carbon donates a pair of electrons to the vacant orbital of the metal. A π bond is formed by the donation of a pair of electrons from the filled metal *d* orbital to the vacant antibonding π*. The σ bond strengthens the π bond and vice versa. Thus a synergic effect is produced due to this metal-to-ligand bonding. The synergy strengthens the bond between CO and the metal.

The appearance of a hydroxyl group (formation of acetoin) not only leads to decreased strength of the metal–molecule bond due to the removal of the carbonyl group but also to a greater affinity for the solvent due to hydrogen bonding to similar OH groups in the isopropyl alcohol solvent molecules. This greater affinity for the solvent would decrease the relative affinity for the catalyst surface. The rapid desorption of acetoin from the surface of Pd would drastically decrease the possibility of the consecutive hydrogenation of acetoin to butanediol that easily occurs in other systems.[2,37]

The strong adsorption of 2,3-butanedione was clearly visible in the reaction series with variable values of the initial *DC* concentration. Higher values decreased the reaction rate drastically.

The weak adsorption of hydrogen on palladium in these reaction experiments could have been enhanced by the electrodeficient state of the metal particles. Singh and Vannice[38] noted that hydrogen adsorption is weak over $Pd^{\delta+}$ due to the depletion of *d* electrons by adjacent electronegative species.

The best fit model, the two-step reaction of hydrogen addition to the carbonyl group, has been proposed by several researchers.[26,39,40] Particularly in this case the rate-limiting step seemed to be the insertion of the first hydrogen. The reasons for the onset of such a reaction path for the Pd/BTAl-2,3-butadione system can be many: (i) the electrodeficiency of Pd reduces the equilibrium concentration of available surface atomic hydrogen and slows down the hydrogenation steps; (ii) the presence of a protic solvent favors the formation of a low energy, half-hydrogenated, hydroxyalkyl intermediate; (iii) pairwise addition of two hydrogen atoms is not possible due to a scarcity of adjacent sites suitable for hydrogen chemisorption.[41]

From a simpler point of view the selectivity to the intermediate in the chain reaction series of Fig. 1 is also partly influenced by the intrapellet diffusion resistance. Early studies on the selectivity of these systems indicate that the selectivity to the first product (acetoin) is favored by the onset of a reaction pattern under chemical control, while the second product (butanediol) is favored by the appearance of strong intrapellet diffusional limitations.[42] The use of an efficient egg-shell catalyst of thin metal layer thickness as that used in this work should contribute to the selectivity to acetoin. In any case, the selectivity to acetoin over the 0.3PdBTAl catalyst was practically 100% at the reaction conditions used in this work.

ACKNOWLEDGEMENTS

The technical assistance of C. Mázzaro and the financial assistance of CONICET, UNL and SECTeI are greatly acknowledged.

REFERENCES

1 Rylander PN, *Hydrogenation Methods*. Best Synthetic Methods Series, Academic Press Inc. (London) Ltd, 70–71 (1985).
2 Li V and Liu HF, Modification of metal complex on the stereoselective hydrogenation of 2,3-butanedione. *Chinese Chem Lett* **12**:127–128 (2001).
3 Zuo X, Li Y and Liu H, Modification effect of metal cations on the stereoselective hydrogenation of 2,3-butanedione. *Catal Lett* **71**:177–180 (2001).
4 Bartowsky EJ and Henschke PA, The 'buttery' attribute of wine - diacetyl - desirability, spoilage and beyond. *Int J Food Microbiol* **96**:235–252 (2004).
5 Calbert HE and Price WV, A study of the diacetyl in cheese. I. Diacetyl content and flavor of cheddar cheese. *J Dairy Sci* **32**:515–520 (1949).
6 Whittaker P, Clarke JJ, San RHC, Begley TH and Dunkel VC, Evaluation of the butter flavoring chemical diacetyl and a fluorochemical paper additive for mutagenicity and toxicity using the mammalian cell gene mutation assay in L5178Y mouse lymphoma cells. *Food Chem Toxicol* **46**:2928–2933 (2008).

7 Safety and Health Information Bulletin (SHIB) 10-14-2010, US Department of Labor, Occupational Safety and Health Administration, Directorate of Technical Support and Emergency Management, Office of Science and Technology Assessment.
8 Badano JM, Betti C, Rintoul I, Vich-Berlanga J, Cagnola E, Torres G, Vera C, Yori J and Quiroga M, New composite materials as support for selective hydrogenation; egg-shell catalysts. *Appl Catal A: Gen* **390**:166–174 (2010).
9 Studer M, Okafor V and Blaser HU, Hydrogenation of butane-2,3-dione with heterogeneous cinchona modified platinum catalysts: a combination of an enantioselective reaction and kinetic resolution. *Chem Commun* 1053–1054 (1998).
10 Froment GF and Bischoff KB, *Chemical Reactor Analysis and Design*. Wiley Series in Chemical Engineering (1979).
11 Bertero NM, Trasarti AF, Apesteguía CR and Marchi AJ, Solvent effect in the liquid-phase hydrogenation of acetophenone over Ni/SiO^2: a comprehensive study of the phenomenon. *Appl Catal A: Gen* **394**:228–238 (2011).
12 Fogler HS, *Elementos de Ingeniería de las Reacciones Químicas*, 3rd edn. Prentice-Hall, Pearson Educación, 758–761 (2001).
13 NIST, X-ray Photoelectron Spectroscopy Database NIST Standard Reference Database 20, Version 3.5 (Web Version). National Institute of Standards and Technology, USA (2007).
14 Bozon-Verduraz F, Omar A, Escard J and Pontvianne B, Chemical state and reactivity of supported palladium: I.Characterization by XPS and uv-visible spectroscopy. *J Catal* **53**:126–134 (1978).
15 Fígoli NS, L'Argentiere PC, Arcoya A and Seoane XL, Odification of the properties and sulfur resistance of a Pd/SiO2 catalyst by La addition. *J Catal* **155**:95–105 (1995).
16 Gaspar AB, dos Santos GR, de Souza-Costa R and da Silva MAP, Hydrogenation of synthetic PYGAS-effects of zirconia on Pd/Al_2O_3. *Catal Today* **133**:400–405 (2008).
17 NIST 69 Standard Reference Database, NIST Chemistry Webbook.
18 Bennett JA, Creamer NJ, Deplanche K, Macaskie LE, Shannon IJ and Wood J, Palladium supported on bacterial biomass as a novel heterogeneous catalyst: a comparison of Pd/Al_2O_3 and bio-Pd in the hydrogenation of 2-pentyne. *Chem Eng Sci* **65**:282–290 (2010).
19 Semagina N, Renken A and Kiwi-Minsker L, Monodispersed Pd-nanoparticles on carbon fiber fabrics as structured catalyst for selective hydrogenation. *Chem Eng Sci* **62**:5344–5348 (2007).
20 Gallezot P, Hydrogenation – heterogeneous, in *Encyclopedia of Catalysis*, Vol **4**, ed by Horvath IT. John Wiley & Sons (2003).
21 Horiuti J and Polanyi M, Exchange reactions of hydrogen on metallic catalysts. *Trans Faraday Soc* **30**:1164–1172 (1934).
22 Tanaka K, Adsorption and Hydrogenation of Carbonyl and Related Compounds on Transition Metal Catalysts, in *Catalytic Hydrogenation*, Volume **27**, ed by Cervený L. Chapter 3, Elsevier (1986).
23 Tanaka K, Hydrogenation of carbonyl compounds on transition metal catalysts. *Hyomen* **18**:245–259 (1980).
24 Blyholder G and Neff LD, Structure of surface species on cobalt. *J Phys Chem* **70**:3494–3496 (1969).
25 Desai SK, Pallassana V and Neurock M, A periodic density functional theory analysis of the effect of water molecules on deprotonation of acetic acid over Pd(111). *J Phys Chem B* **105**:9171–9182 (2001).
26 Vidal S, Masson J, Court J, and Cividino P, Kinetics of the liquid phase hydrogenation of citronellol over Raney nickel catalyst. *J Chim Phys* **92**:2060–2074 (1995).
27 Ronchin L, Vavasori A, Bernardi D, Cavinato G and Toniolo L, Selective hydrogenation of ethyl-benzoylacetate to 3-hydroxy-3-phenyl-propionate catalyzed by Pd/C in EtOH as a solvent in the presence of KOH: the role of the enolate ion on the reaction mechanism. *Appl Catal A: Gen* **355**:50–60 (2009).
28 Katayama T and Nitta T, Solubilities of hydrogen and nitrogen in alcohols and n-hexane. *J Chem Eng Data* **21**:194–196 (1976).
29 Safamirzaei M, Modarress H and Mohsen-Nia M, Modeling the hydrogen solubility in methanol, ethanol, 1-propanol and 1-butanol. *Fluid Phase Equilibria* **289**:32–39 (2010).
30 Vicente J, d'Angelo H and Francesconi AZ, Gas–liquid solubility of hydrogen in n-alcohols ($1 \leq n \leq 4$) at pressures from 3.6 MPa to 10 MPa and temperatures from 298.15 K to 525.15 K. *J Chem Eng Data* **46**:671–674 (2001).
31 Descamps C, Coquelet C, Bouallou C and Richon D, Solubility of hydrogen in methanol at temperatures from 248.41 to 308.20 K. *Thermochim Acta* **430**:1–7 (2005).
32 Zhou Z, Cheng Z, Cao Y, Zhang J, Yang D and Yuan W, Kinetics of the selective hydrogenation of pyrolysis gasoline. *Chem Eng Technol* **30**:105–111 (2007).
33 Zhou Z, Zeng T, Cheng Z and Yuan W, Kinetics of selective hydrogenation of pyrolysis gasoline over an egg-shell catalyst. *Chem Eng Sci* **65**:1832–1839 (2010).
34 Crespo-Quesada M, Grasemann M, Semagina N, Renken A, and Kiwi-Minsker L, Kinetics of the solvent-free hydrogenation of 2-methyl-3-butyn-2-ol over a structured Pd-based catalyst. *Catal Today* **147**:247–254 (2009).
35 Efremenko I, Implication of palladium geometric and electronic structures to hydrogen activation on bulk surfaces and clusters. *J Mol Catal A: Chem* **173**:19–59 (2001).
36 Conrad H, Ertl G and Latta EE, Adsorption of hydrogen on palladium single crystal surfaces. *Surf Sci* **41**:435–446 (1974).
37 Slipszenko J, Griffiths S, Johnston P, Simons K, Vermeer W and Wells P, Enantioselective hydrogenation: V. Hydrogenation of butane-2,3-dione and of 3-hydroxybutan-2-one catalysed by cinchona-modified platinum. *J Catal* **179**:267–276 (1998).
38 Singh UK and Vannice MA, Kinetics of liquid-phase hydrogenation reactions over supported metal catalysts – a review. *Appl Catal A: Gen* **213**:1–24 (2001).
39 Sachtler WMH and Huang YY, Metal/overlayer and encaged carbonyl cluster catalysis. *Appl Catal A: Gen* **191**:35–44 (2000).
40 Sinha NK and Neurock M, A first principles analysis of the hydrogenation of C1-C4 aldehydes and ketones over Ru(0 0 0 1). *J Catal* **295**:31–44 (2012).
41 Taskinen A, Molecular modeling of asymmetric induction in heterogeneously catalyzed hydrogenation of the C=O bond. Doctoral thesis, Abo Akademi University, Turku, Finland (2010).
42 Levenspiel O, *Chemical Reaction Engineering*, 3rd edn. Wiley (1998).

